

# Quantification of Extracellular DNA Network Abundance and Architecture within Streptococcus gordonii Biofilms Reveals Modulatory Factors

**DOI:**
10.1128/aem.00698-22

# Quantification of eDNA network abundance and architecture within *Streptococcus gordonii* biofilms reveals modulatory factors

H. J. Serrage[1], D. Alibhai[2], S. Cross[2], N. Rostami[3], A. A. Jack[1], C. R. Lawler[1], N. S. Jakubovics[3], M. A. Jepson[2] and A. H. Nobbs[1]*

Bristol Dental School, University of Bristol, Bristol, UK[1]

Wolfson Bioimaging Facility, Biomedical Sciences Building, University of Bristol, Bristol, UK[2]

School of Dental Sciences, Newcastle University, Newcastle upon Tyne, UK[3]

Corresponding author details*: Angela.Nobbs@bristol.ac.uk

Email address: hannah.serrage@bristol.ac.uk

Address: Bristol Dental School, Lower Maudlin Street, Bristol BS1 2LY, UK

## Abstract

Extracellular DNA (eDNA) is an important component of biofilm matrix that serves to maintain biofilm structural integrity, promotes genetic exchange within the biofilm, and provides protection against antimicrobial compounds. Advances in microscopy techniques have provided evidence of the cobweb- or lattice-like structures of eDNA within biofilms from a range of environmental niches. However, methods to reliably assess the abundance and architecture of eDNA remain lacking. This study aimed to address this gap by development of a novel, high-throughput image acquisition and analysis platform for assessment of eDNA networks *in situ* within biofilms. Utilising *Streptococcus gordonii* as the model, the capacity for this imaging system to reliably detect eDNA networks and monitor changes in abundance and architecture (e.g., strand length, branch number) was verified. Evidence was provided of the capacity for glucans to stabilise eDNA matrices, while it was revealed that surface-bound nuclease SsnA could modify these structures under conditions permissive for enzymatic activity. Moreover, cross-talk between the competence and hexa-heptapeptide permease systems was shown to regulate eDNA release by *S. gordonii.* This novel imaging system can be applied across the wider field of biofilm research, with potential to significantly advance interrogation of the mechanisms by which the eDNA network architecture develops, how it can influence biofilm properties, and how it may be targeted for therapeutic benefit.

## Importance

As part of biofilm development, bacteria produce and encase themselves within a rich matrix abundant in extracellular DNA (eDNA), which has proven important in the maintenance of the structural integrity of many microbial biofilms. eDNA is released from bacterial cells via lysis or active secretion to form lattice like networks stabilised by DNA binding proteins. However, our knowledge and targeting of eDNA is currently hindered by a lack of tools for the quantitative assessment of eDNA networks within biofilms. Here, we demonstrate use of a novel image acquisition and analysis platform with the capacity to reliably monitor the abundance and architecture of eDNA networks. Exploitation of this tool provided insight into the complex modulation of eDNA networks within *S. gordonii* biofilm. Indicative of the potential of this tool to significantly advance our understanding of how eDNA networks are formed within biofilms, their regulation and how best they might be manipulated.

## Introduction

Biofilm development is characterised by the production and release of extracellular polymeric substance (EPS) to form a matrix that encases the microbial community. EPS accounts for >90% biofilm dry weight and comprises a rich tapestry of components including extracellular DNA (eDNA), which has been found as a common component of biofilms across a range of environments (1-3). Diverse roles have been ascribed to eDNA, including maintenance of biofilm structural integrity, facilitating initial adhesion to surfaces, acting as a reservoir for genetic exchange, providing protection against antimicrobial compounds, and as a nutrient source (4). As a consequence, eDNA is often considered an attractive target for the management of biofilms, which account for up to 80% of all nosocomial infections in humans (5).

Within the biofilm, eDNA is proposed to conform to an “electrostatic net” model where, under low pH conditions, negatively charged eDNA forms electrostatic interactions with positively charged DNA binding proteins within EPS, acting as a net that interconnects cells (6, 7). Advances in techniques for the visualisation of fluorescently stained eDNA networks have provided insights into their structural composition (8-10). Specifically, eDNA has been shown to form Holliday junction-like (9) and G-quadruplex structures (8), stabilised by DNA binding proteins (11-14), that ultimately form cobweb- or lattice-like networks across the biofilm (9, 10). However, understanding of the mechanisms by which eDNA is released, how this is regulated, and the spatiotemporal dynamics of eDNA network formation remains limited. This is, in part, driven by a lack of tools with the capacity to reliably detect and quantify the abundance and architecture of eDNA networks within biofilms.

One ecological niche in which eDNA is recognised as a prominent component of biofilms and a promising therapeutic target is within the oral cavity and, specifically, dental plaque. *Streptococcus gordonii* is a pioneer coloniser and ubiquitous constituent of dental plaque biofilms, where it can influence the accretion of the dental plaque community on salivary pellicle (3, 15). DNA extraction techniques that enable the quantification of soluble eDNA have confirmed the capacity for *S. gordonii* to produce eDNA during biofilm formation (16, 17). From such studies, *S. gordonii* eDNA is hypothesised to be of chromosomal origin and its release has been shown to be hydrogen peroxide ($H_2O_2$) dependent (16, 18). However, further insights into the parameters that may affect *S. gordonii* eDNA networks and their overall architecture are lacking.

Here we demonstrate use of a novel, high-throughput image acquisition and analysis platform to reliably quantify the abundance and architecture of eDNA networks *in situ* within early *S. gordonii* biofilms. By exploiting this technology, these studies provide evidence of glucan stabilisation of the eDNA matrix, reveal that a surface-bound nuclease can modulate the eDNA networks, and identify crosstalk between the competence and hexa-heptapeptide permease (Hpp) systems in regulating eDNA release. The high level detail of eDNA network analysis that this imaging system provides has potential to significantly advance current understanding of biofilm development and manipulation across the spectrum of biofilm research.

## Materials and Methods

### *Bacterial strains and growth conditions*

Bacterial strains utilised in this study are listed in Table 1. *S. gordonii* wild-type and isogenic mutants were routinely cultured in Brain Heart Infusion broth (Lab Neogen) supplemented with 0.5% (w/v) yeast extract (BD; BHY) under stationary conditions for 16 h in a candle jar at 37$^{o}$C. As needed, broth cultures were supplemented with 100 µg/ml spectinomycin (Sp), 1.5 - 5 µg/ml erythromycin (Ery) or 250 µg/ml kanamycin (Kan). A defined medium (YPT) was used for eDNA secretion studies comprising 20 mM $NaH_2PO_4$ (pH 7), 1 x yeast nitrogen base (Difco) and 0.1% (w/v) Bacto-tryptone ± supplementation with 0.2% (w/v) glucose or sucrose (19).

### Mutagenesis of *S. gordonii*

*Streptococcus gordonii* DL1 (Challis) is predicted to express a 779-amino acid protein with 76% homology to streptococcal wall-anchored nuclease (SWAN), a nuclease in *Streptococcus sanguinis* capable of modulating the eDNA of neutrophil extracellular traps (20). The gene encoding this protein, designated streptococcal surface nuclease A (*ssnA*), was deleted by allelic exchange. In brief, flanking regions of *ssnA* were amplified by PCR using primer pairs SsnA.F1/R1 and SsnAF2/R2 (Table 2), while the *aad9* spectinomycin resistance cassette was amplified from plasmid pFW5 using SsnA.aad9F/R (Table 2)(21). Amplicons were joined by overlapping PCR using primers SsnA.F1/R2 (Table 2), yielding a final amplicon of 1936 bp. This was transformed into wild-type *S. gordonii* and successful mutagenesis confirmed by sequencing.

A similar allelic exchange approach was used to generate a Δ*comDE* mutant using primer pairs ComCD.F1/ComDE.R1 and ComDE.F1/ComCDE.R2 to amplify the upstream (884 bp) and downstream (619 bp) flanking regions, respectively, and primers Aad9.F/Aad9.R to amplify *aad9* from pFW5 (Table 2). Likewise, a Δ*comR1*/*R2* mutant was generated using primer pairs ComR1.F1/R1 with ComR1.F2/R2 or ComR2.F1/R1 with ComR2.F2/R2 to amplify the flanking regions of *comR1* or *comR2*, respectively (Table 2). These were joined to the *aad9* cassette from pFW5 (21) or the *ermAM* erythromycin resistance cassette from plasmid pVA838 (22) using primers aad.ComR1.F/aad.ComR1.R or ermAM.ComR2.F/ermAM.ComR2.R, respectively (Table 2). The *hppA* gene was inactivated by allelic exchange with *ermAM* using primers hppA.F1/hppA.R1, hppA.F2/hppA.R2 and ermAM.hppAF/ermAM.hppAR (Table 2). The *hppH* gene was inactivated by allelic exchange with the *aphA3* kanamycin resistance cassette from plasmid pDL276 (23) using primers hppH.F1/hppH.R1, hppH.F2/hppH.R2 and aphA3.hppH.F/aphA3.hppH.R (Table 2). Final amplicons were transformed into wild-type *S. gordonii*. Those for *hppA* and *hppH* were additionally transformed into *S. gordonii* Δ*comCDE* (24).

***Preparation of saliva***

Unstimulated whole saliva was collected on ice and pooled from a minimum of 5 healthy adult donors who provided written consent (approved by the National Research Ethics Committee Central Oxford C;08/H606/87). Pooled saliva was treated with 2.5 mM dithiothreitol (DTT), incubated on ice for 10 min and centrifuged at 10,000 *g* for 10 min to sediment mucins and bacteria. The supernatant was transferred to sterile plasticware, diluted to 10% with distilled water and sterilised through a 0.45 μm filter.

### *Biofilm formation*

Black, clear bottom 24-well plates (Sensoplate™, Greiner Bio-one) were incubated with 10% saliva (500 µl) for 16 h at 4°C. Overnight broth cultures of *S. gordonii* were harvested (5000 *g*, 7 min) and resuspended to $OD_{600}$ 0.25 in YPT-glucose (equivalent to approximately $2.5x10^6$ CFU/ml). Saliva was aspirated from the plates, wells inoculated with 500 µl bacterial suspension and plates incubated in a humid environment at 37°C under gentle agitation (50 rpm) for up to 24 h. Following incubation, non-adherent cells were aspirated, the biofilms washed twice with YPT and either fixed with 4% (w/v) paraformaldehyde (PFA) for 16 h at 4°C for microscopy or resuspended in PBS for alternative applications. For some studies, bacterial suspensions were treated with dextranase (10 µg/ml; Sigma-Aldrich), DNase I (10-25 µg/ml, Sigma-Aldrich), or competence stimulating peptide (CSP, DVRSNKIRLWWENIFFNKK, 10 µg/ml; GenicBio) following inoculation of the plates. To measure glucan levels within the biofilm, dextran Alexa Fluor™ 647 conjugated antibody (1 µM, ThermoFisher Scientific) was applied alongside the bacterial suspension, following 5h incubation wells were washed twice with YPT and fluorescence levels (ex/em: 650/668) measured with a plate reader (Infinite F200 Pro, Tecan). For assessment of biomass, biofilms were stained with 0.5% (w/v) crystal violet, washed with PBS to remove excess stain, and then biomass quantified by release of stain using 10% (v/v) glacial acetic acid and measurement of absorbance at $A_{595}$.

### *Soluble eDNA extraction and quantification*

Biofilms from quadruplicate wells were collected into PBS and the soluble fraction recovered following centrifugation. Fractions were treated at 37 $^{o}$C for 1 h with proteinase K (5 µg/ml; Sigma-Aldrich) and then the eDNA extracted using phenol:chloroform:isoamyl alcohol (25:24:1). The aqueous phase was collected, mixed with 3 M sodium acetate and isopropanol, and incubated for 1 h at 20$^{o}$C. DNA was precipitated and resuspended in $dH_2O$. DNA concentration and quality was then assessed by measurement at $A_{260}/A_{280}$.

### *High-throughput eDNA image capture and analysis*

Following PFA fixation of biofilms, 2% (w/v) bovine serum albumin (Sigma-Aldrich), mouse anti-dsDNA antibody (ab27156, Abcam, 1:1000) and AlexaFluor-594®-conjugated secondary antibody (1:1000) were applied sequentially for 45 mins each. A 20x magnification lens (HC PL APO 20x/0.75 CS2) on a Widefield Leica DMi600 microscope (Leica) coupled to a Photometrics Prime 95B cMOS camera (1200x1200, 11µm pixels, 8 bit, Photometrics) was employed to capture eDNA images using Leica acquisition software (LASX, Leica). eDNA structures were visualised using a cube consisting of a 560/40 nm excitation filter, 595 nm LP dichroic and 645/76 nm emission filter at an exposure time of up to 100 ms. Positions within each well were defined automatically using a custom-made MATLAB (Mathworks) programme which generated xyz positions to be used within the ‘mark and find’ function of LASX, facilitating the acquisition of at least 6 images per well. Each image covered an area of 660 x 660 µm and all images were taken in the same position in each well. All images were acquired

as 10 µm Z-stacks (13 slices x 0.8 µm steps) to ensure images of eDNA at the optimum focus level were taken. Glucans within biofilm were visualised in a similar manner using a cube consisting of a 620/60 nm excitation filter, 660 nm LP dichroic and 700/38 nm emission filter.

Quantification of eDNA networks was performed using the Wolfson Bioimaging Facility modular image analysis Fiji plugin, MIA (25-27). Initially, eDNA was segmented from fluorescence images using 2D ridge detection (28, 29). Small gaps between proximal eDNA ends were then bridged, subject to user-defined alignment filters (end-end distance and maximum angular difference). Finally, length and branching metrics for the eDNA structures were obtained using the Analyze Skeleton plugin (30). Structural composition and abundance of eDNA were then assessed using Excel software (Microsoft).

***Statistical analyses***

Data were processed utilising Excel software (Microsoft) and analyses were performed using Prism (GraphPad Software, California, US). All experiments were performed at least in triplicate, unless otherwise stated, and data were analysed using Student's *t*-test (when comparing two groups) or general linear model (GLM) followed by one-way ANOVA and Tukey test (when comparing three or more groups).

## Results

### *Evaluation of eDNA production in early-stage S. gordonii biofilms*

Pilot studies had indicated the capacity for *S. gordonii* to produce an eDNA network during biofilm formation, alike in architecture to the yarn-like eDNA structures produced by *Enterococcus faecalis* biofilms (10). *S. gordonii* biofilms were therefore selected as the model to verify the capacity for our image analysis approach to reproducibly quantity eDNA networks *in situ* within biofilms. Before such studies could be undertaken, however, it was necessary to establish the optimal stage during biofilm development at which *S. gordonii* produces eDNA. Previous reports had indicated that *S. gordonii* releases eDNA during early biofilm formation (16, 17) but detailed, time dependent changes in eDNA release were lacking. Phenol:chloroform:isoamyl DNA extraction was combined with crystal violet staining to systematically evaluate changes in soluble eDNA and biomass quantities over time. A time-dependent increase in eDNA concentration was seen that peaked at 5 h and then began to decline, while biomass levels continued to increase beyond 5 h (Fig. 1). This indicated that eDNA levels did not simply correlate with *S. gordonii* cell numbers. As it represented the peak for eDNA concentration, a 5-h time point was selected to further evaluate eDNA within *S. gordonii* biofilms.

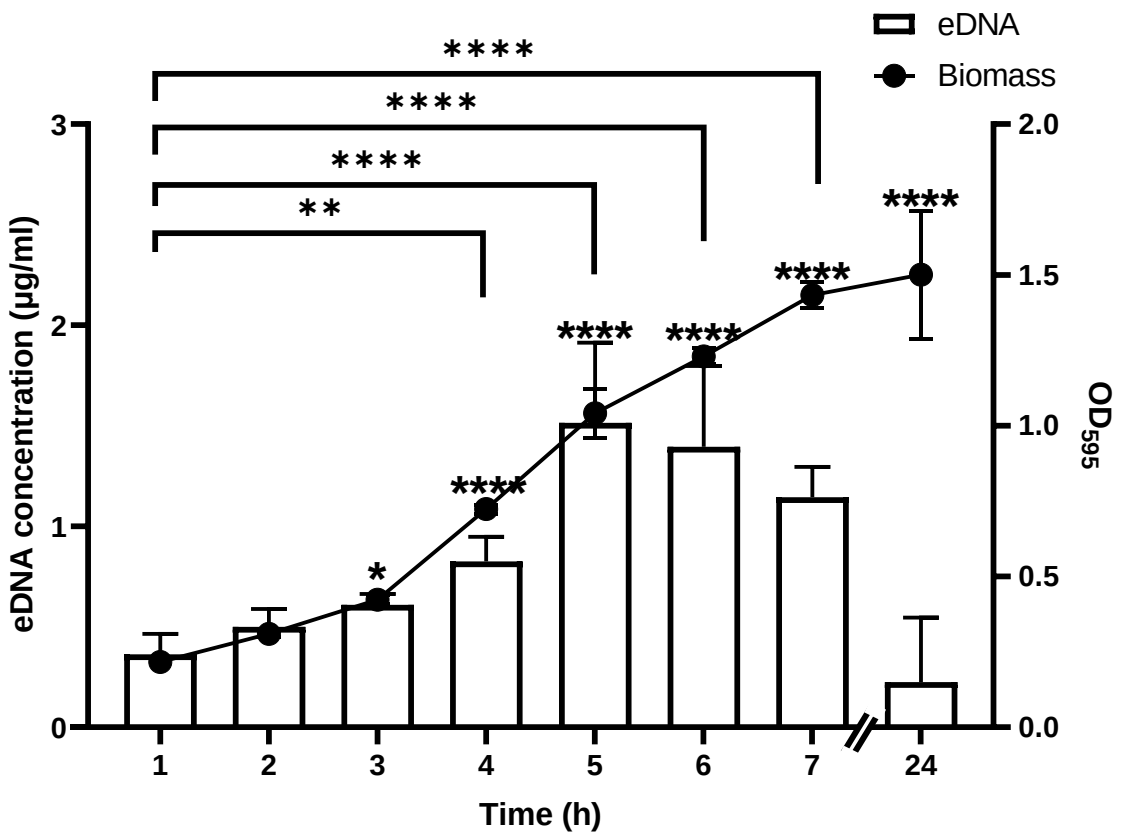


**Figure 1: Changes in *S. gordonii* biofilm biomass and eDNA over time.** WT *S. gordonii* biofilms were grown at 37 °C in YPTG on saliva-coated 24-well plates for up to 24 h and levels of biomass determined by crystal violet staining (line) or eDNA assessed using the phenol:chloroform:isoamyl DNA extraction method (columns). Data are presented as mean values ± SD. *P< 0.05, **P< 0.01 or ****P< 0.0001 compared to 1 h value as determined by one-way ANOVA followed by post-hoc Tukey Test (n=3).

### *Quantification of eDNA networks within S. gordonii biofilms*

The quantification of DNA by phenol:chloroform:isoamyl alcohol extraction has been used widely to quantify levels of eDNA within biofilms (31-33). However, this approach only indicates the concentration of soluble eDNA and can provide no information on the structural complexity of eDNA within the biofilm architecture. To validate a system for the reliable detection of eDNA matrices, following biofilm culture of FITC-stained *S.*

gordonii, eDNA matrices were fluorescently labelled. This technique provided indication of the cobweb like interwoven eDNA networks across *S. gordonii* biofilm (Figure 2x). Subsequently, a novel mass image acquisition and high-throughput image analysis system was devised to quantify these eDNA networks *in situ* within biofilms. Following immunolabelling, web- or constellation-like structures of eDNA could be visualised within *S. gordonii* biofilms (Fig. 2A). Our image analysis software could then be exploited to detect and quantify these eDNA structures (Fig. 2B). Due to differences in pixel density between the background of the image and eDNA matrices, our software was able to reliably detect and subsequently highlight eDNA structures with various colours to indicate different points of origin of each eDNA structure. Information regarding their quantity and architecture was then output. Specifically, data could be obtained regarding the total percentage of each field of view comprising eDNA, total eDNA stranding (μm/mm², total length of eDNA strands per mm²), average branch length (μm) and average number of eDNA branches diverging from a single point (number of junctions/number of branches per junction). To test this analysis capability, whilst verifying the accuracy and sensitivity of this imaging approach in detecting eDNA, studies were repeated in the presence of an increasing concentration (10–25 μg/ml) of DNase I. As was anticipated, a significant reduction in eDNA levels was seen (Fig. 3A). This was reflected in the quantification, as % field of view comprising eDNA networks (Fig. 3B) and total eDNA stranding (Fig. 3C) were significantly diminished following DNase I application. Variations in eDNA architecture could also be measured. The average number of eDNA branches reduced with increasing DNase I concentration (Fig. 3F), likely correlated with the general reduction in eDNA levels, but no significant effect

255 on average branch length (Fig. 3D) or eDNA junction structure (Fig. 3E,G) was seen.
256 Together, these data provided confidence that the imaging system could accurately
257 detect eDNA networks within biofilms and provide information relating to both quantities
258 of eDNA and the overall architecture of the eDNA networks. These data also implied
259 that DNase I could drive the removal and/or release of eDNA, thus reducing bulk
260 quantity, but did not significantly impact its fundamental organisation.

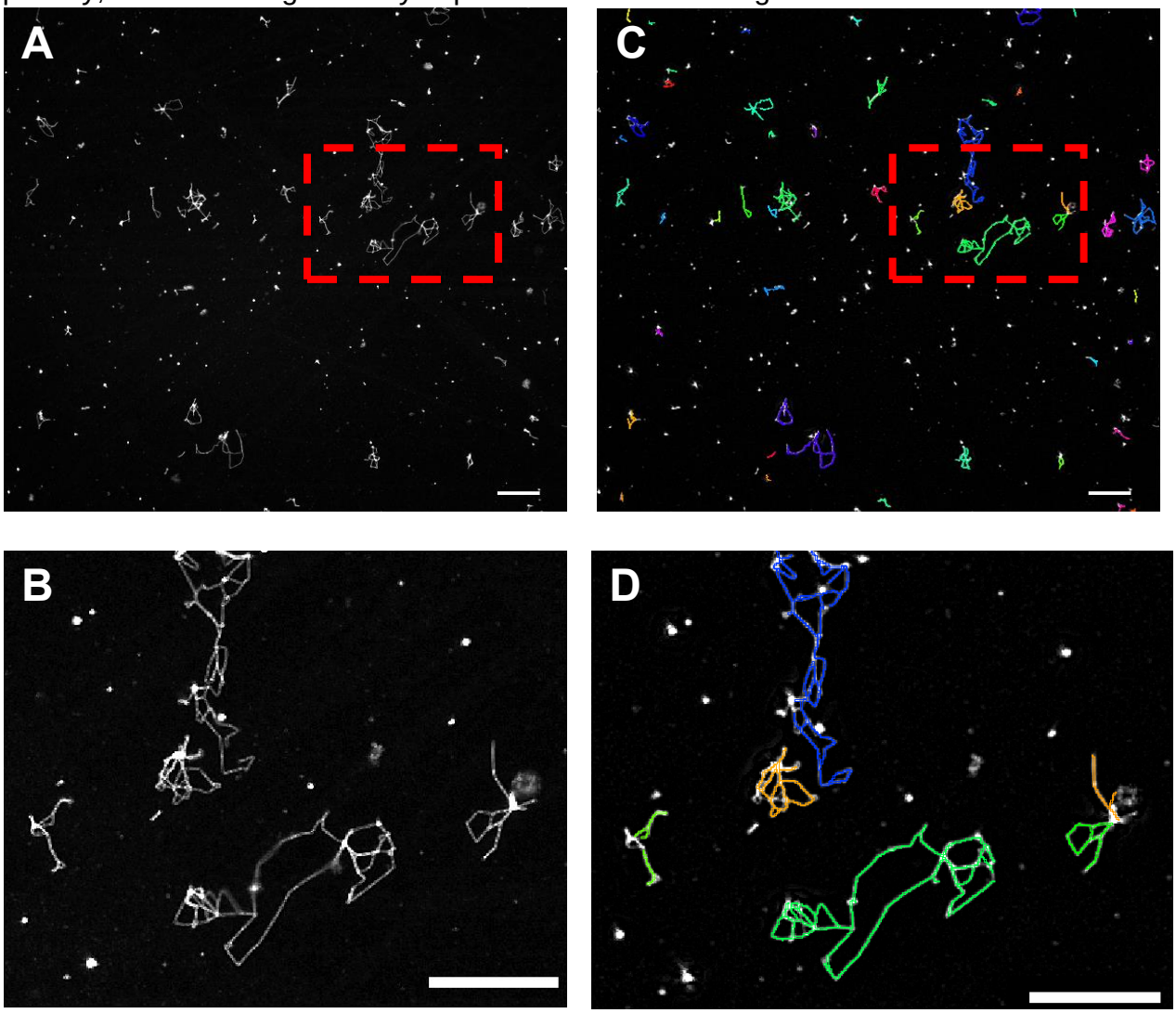


**Figure 2:** Visualization of eDNA in S. gordonii biofilms at 5 h. WT S. gordonii biofilms were grown at 37 °C in YPTG on saliva-coated 24-well plates for 5 h. Networks of eDNA were then immunolabelled and visualized by widefield microscopy (A, B). Image analysis software was used to detect and quantify eDNA strands, as shown in (C, D). Representative images are shown. Scale bars, 50 µm.

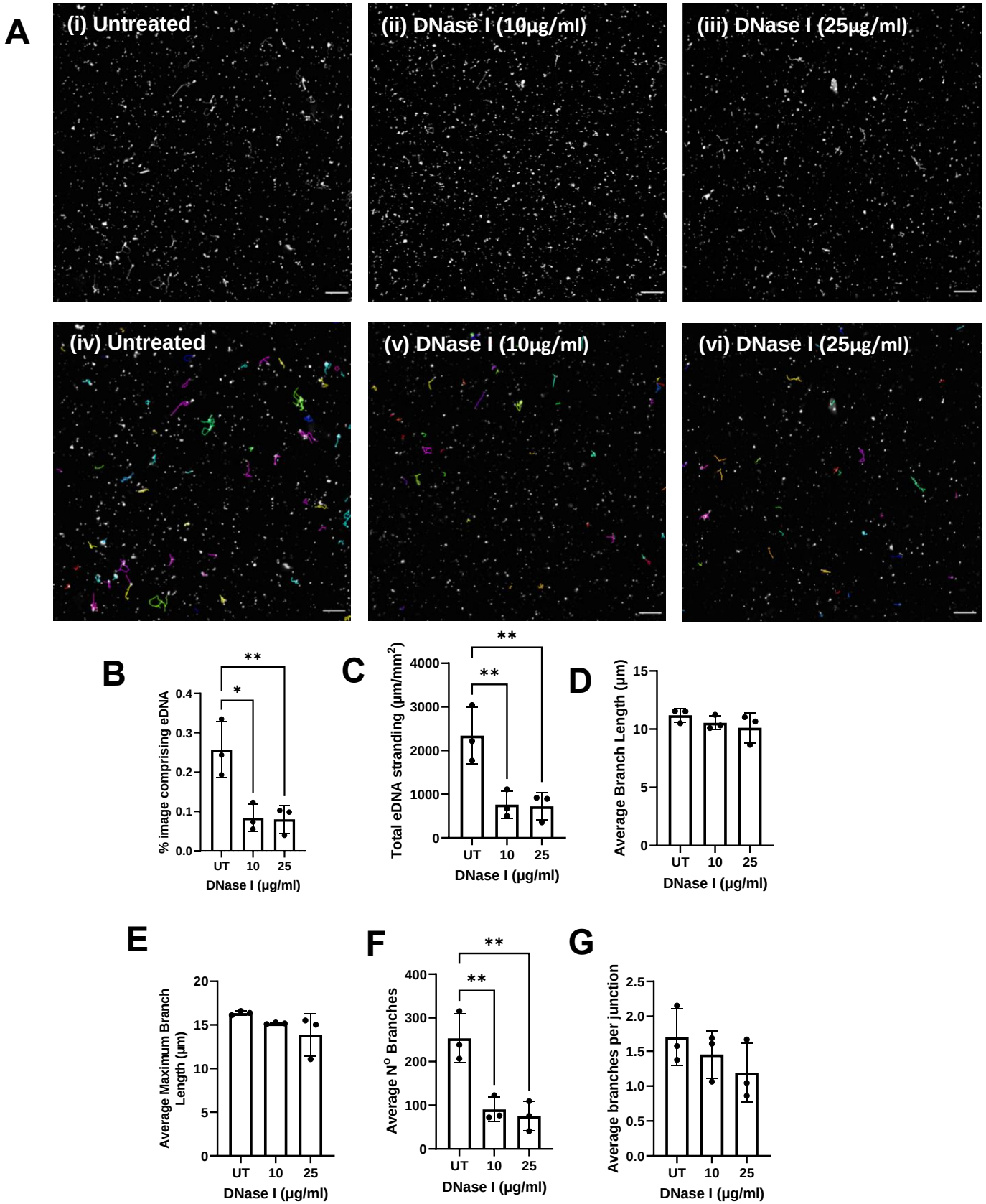
A
(i) Untreated
(ii) DNase I (10µg/ml)
(iii) DNase I (25µg/ml)
(iv) Untreated
(v) DNase I (10µg/ml)
(vi) DNase I (25µg/ml)
B
% image comprising eDNA
0.0
0.1
0.2
0.3
0.4
UT
10
25
DNase I (µg/ml)
**
*
C
Total eDNA stranding (µm/mm²)
0
1000
2000
3000
4000
UT
10
25
DNase I (µg/ml)
**
**
D
Average Branch Length (µm)
0
5
10
15
UT
10
25
DNase I (µg/ml)
E
Average Maximum Branch Length (µm)
0
5
10
15
20
UT
10
25
DNase I (µg/ml)
F
Average N° Branches
0
100
200
300
400
UT
10
25
DNase I (µg/ml)
**
**
G
Average branches per junction
0.0
0.5
1.0
1.5
2.0
2.5
UT
10
25
DNase I (µg/ml)

261

**Figure 3: eDNA detection and quantification following DNase I treatment.** WT *S. gordonii* biofilms were grown at 37 °C in YPTG ± 10-25 µg/ml DNase I on saliva-coated 24-well plates for 5 h. Networks of eDNA were then immunolabelled and visualized by widefield microscopy (A, i - iii) and image software used to detect eDNA networks (A, iv – vi). Quantifiable differences in the % of field of view comprising eDNA (B), total eDNA stranding per $mm^2$ (C) , average eDNA branch length (D), average maximum eDNA branch length (E), average number of branches per field of view (F) and average number of junctions per eDNA structure (G) were then assessed using Excel. Data are presented as mean ± SD.**P<0.01, *P<0.05 relative to untreated (UT) control, as determined via one-way ANOVA followed by Tukey test (n = 3). Scale bars, 50 µm.

### ***Effects of carbon source on eDNA networks***

Having confirmed the capacity for the imaging system to reliably detect and analyse eDNA networks, the next step was to exploit this approach to gain an improved understanding of eDNA within *S. gordonii* biofilms. For this work, a series of parameters were selected that had previously been implicated in modulating eDNA. The first of these was the effect of sugars. Prior studies had identified carbon catabolite dependent modulation of eDNA release in *S. gordonii* and *S. sanguinis* biofilms (34-36), and sucrose has been shown to promote eDNA dependent *S. mutans* biofilm formation, in which glucans were proposed to stabilise the eDNA matrices (37), (38). To validate whether the same trend could be observed within *S. gordonii* biofilms, our imaging system was exploited to examine the differential effects of glucose and sucrose on *S. gordonii* total eDNA stranding levels (Fig. 4A). Levels of eDNA for biofilms cultured in sucrose were 69% higher than those observed for glucose-cultured biofilms (Fig. 4b), while biomass levels differed by only 13% (Fig. 4C). Application of dextranase to both

277 glucose and sucrose biofilms resulted in modulation of eDNA matrix architecture (Fig.
278 4E-F).

279 Furthermore, abundance of eDNA in glucose-grown biofilms were unaffected by
280 dextranase, although there was a 25% reduction in biomass (Fig. 4B,C). By contrast, a
281 76% decrease in eDNA levels was observed for the sucrose-grown biofilms following
282 dextranase application, alongside a 25% reduction in biomass (Fig. 4B,C). These data
283 supported a role for glucans in eDNA networks within *S. gordonii* biofilms.

284 To further verify an association between eDNA levels and glucans, an *S. gordonii* Δ*gtfG*
285 mutant was tested. Glucosyltransferase G (GtfG) is the only glucosyltransferase
286 expressed by *S. gordonii,* is located extracellularly and is responsible for the generation
287 of glucans during *S. gordonii* biofilm formation (39). GtfG hydrolyses dietary sucrose,
288 synthesising glucose moieties into glucan polymers with α-1,6 and α-1,3 linkages (40,
289 41). In the presence of glucose, loss of GtfG reduced levels of eDNA by 53% but this
290 effect was much more pronounced in the presence of sucrose, with a reduction of 84%
291 (Fig. 5A,B). No effect was seen on biomass levels upon loss of GtfG with either
292 condition (Fig. 5C), but like dextranase, loss of GtfG resulted in modulation of eDNA
293 matrix architecture within sucrose biofilm (Fig. 5E – F). Finally, to enable glucans to be
294 visualised alongside eDNA, dextran conjugated to Alexa Fluor™ 647 was applied to the
295 biofilms. The fluorescently labelled dextran acts as an acceptor that is incorporated into
296 newly formed glucans by Gtfs. As was expected, sucrose-cultured biofilms exhibited a
297 significantly higher fluorescence output than their glucose-cultured counterparts,
298 confirming a greater abundance of glucans (Fig. 6A). When combined with
299 immunolabelling of eDNA, co-localisation of eDNA structures with glucans could be

observed (Fig. 6B). Taken together, these data suggest a potential synergy between eDNA and glucans during *S. gordonii* biofilm formation, in which the glucans may serve to promote the structural stability of eDNA matrices.

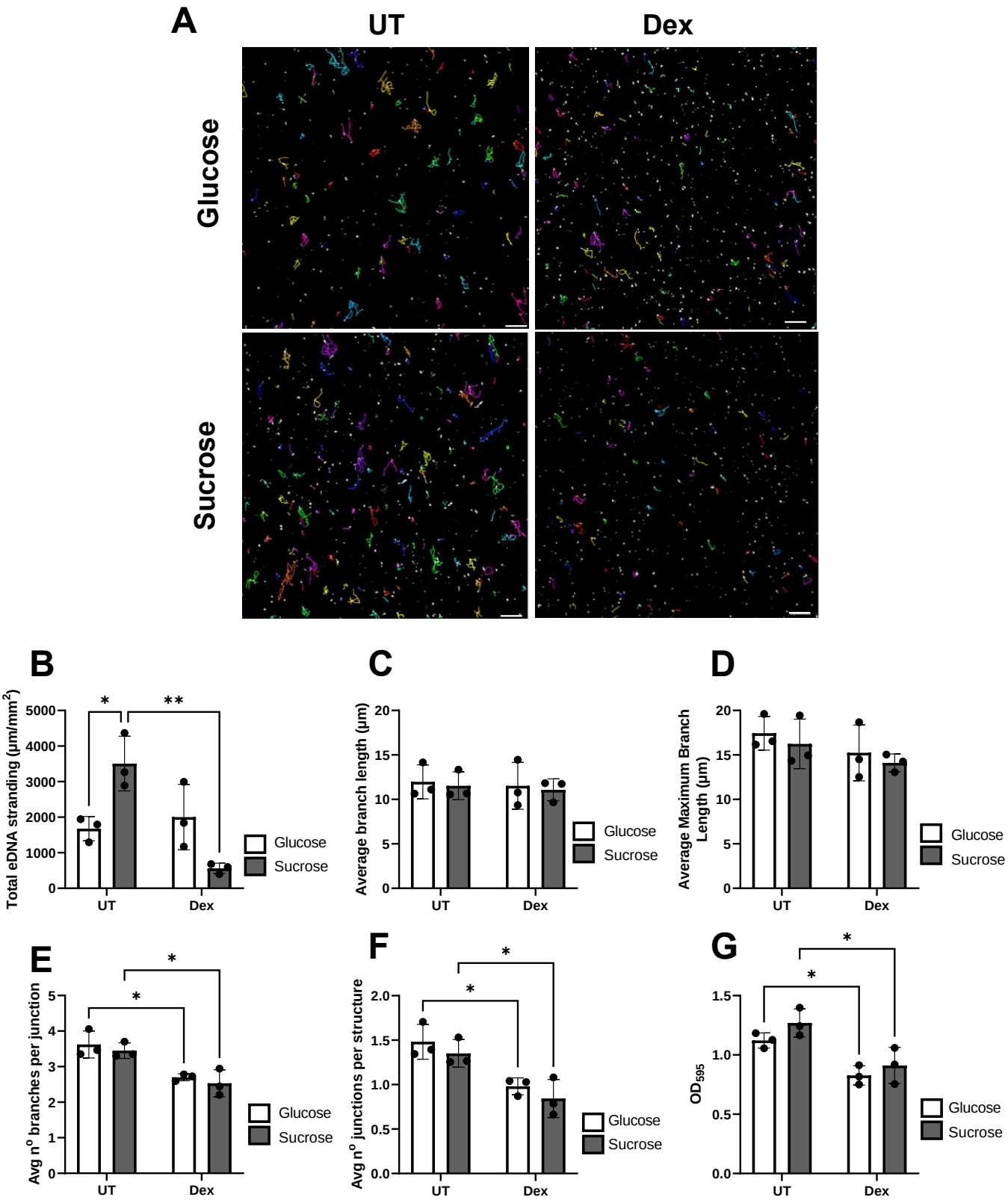
A
UT
Dex
Glucose
Sucrose
B
Total eDNA stranding (µm/mm²)
5000
4000
3000
2000
1000
0
*
**
UT
Dex
Glucose
Sucrose
C
Average branch length (µm)
20
15
10
5
0
UT
Dex
Glucose
Sucrose
D
Average Maximum Branch Length (µm)
20
15
10
5
0
UT
Dex
Glucose
Sucrose
E
Avg n° branches per junction
5
4
3
2
1
0
*
*
UT
Dex
Glucose
Sucrose
F
Avg n° junctions per structure
2.0
1.5
1.0
0.5
0.0
*
*
UT
Dex
Glucose
Sucrose
G
OD595
1.5
1.0
0.5
0.0
*
*
UT
Dex
Glucose
Sucrose

308

**Figure 4:** Glucans enhance eDNA levels within sucrose-grown biofilms. WT *S. gordonii* biofilms were grown on saliva-coated 24-well plates for 5 h at 37 °C in YPT ± 0.2% glucose/sucrose in the absence (UT) or presence of 10 µg/ml dextranase (Dex). eDNA stranding (A, B), eDNA branching (C, D), number of junctions/branches per eDNA structure (E, F) and levels of biomass (G) were then determined by microscopy or crystal violet staining, respectively. Data are presented as mean ± SD. *P<0.05 and ***P<0.001, as determined via one-way ANOVA followed by Tukey test (n = 3).

309

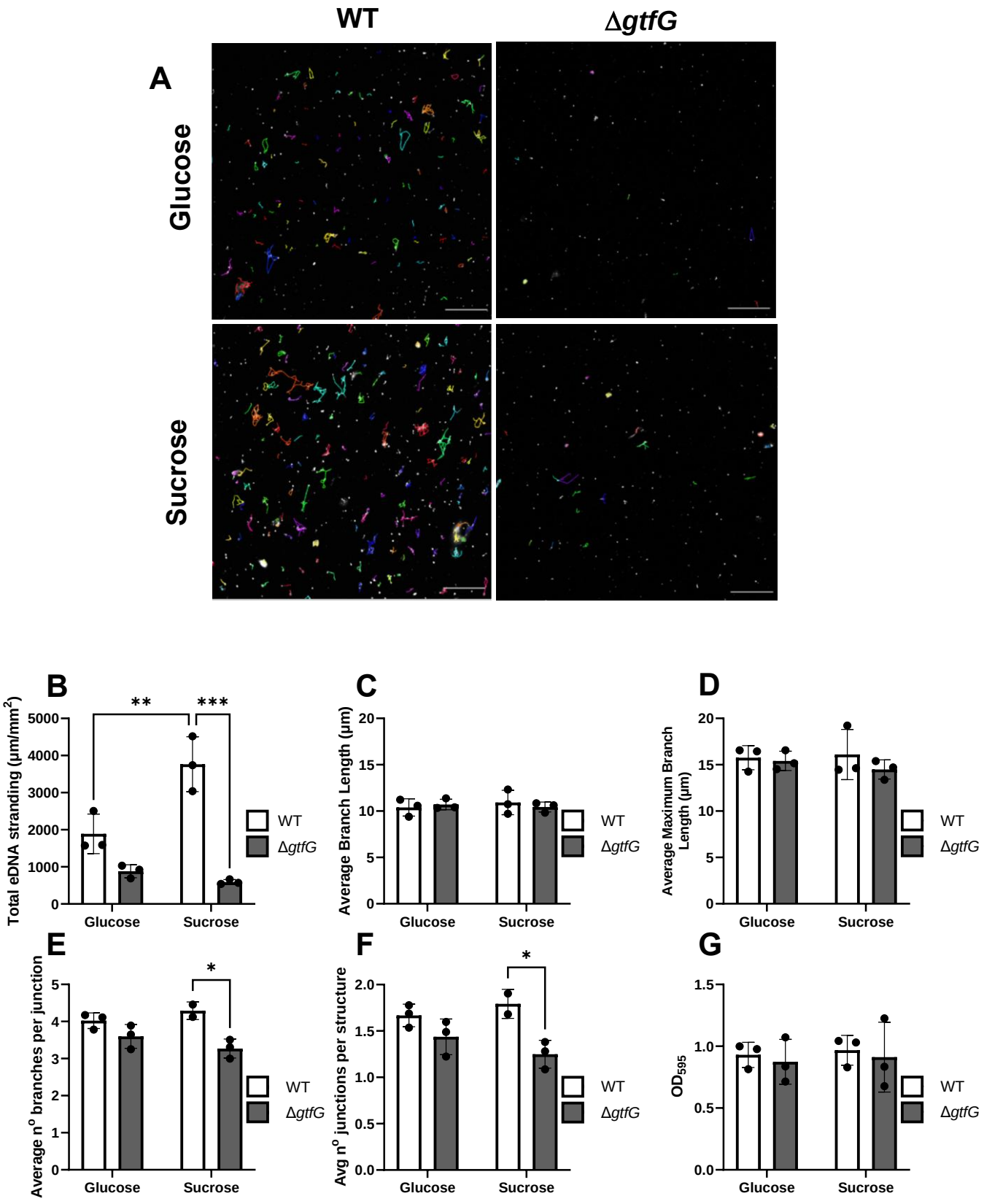
WT
ΔgtfG
A
Glucose
Sucrose
B
Total eDNA stranding (µm/mm²)
**
***
WT
ΔgtfG
Glucose
Sucrose
C
Average Branch Length (µm)
D
Average Maximum Branch Length (µm)
E
Average n° branches per junction
*
F
Avg n° junctions per structure
G
OD595

310

**Figure 5:** Inability to synthesise glucans impairs eDNA levels within biofilms. WT and Δ*gtfG* S. gordonii biofilms were grown for 5 h at 37 °C in YPT ± 0.2% glucose/sucrose. eDNA stranding was assessed via widefield microscopy (A) and quantified (B - F). Levels of biomass (G) were determined by crystal violet staining. Data are presented as mean ± SD. **P<0.01 and ***P<0.001, as determined via one-way ANOVA followed by Tukey test (n = 3). Representative images are shown. Scale bars, 50 µm.

311

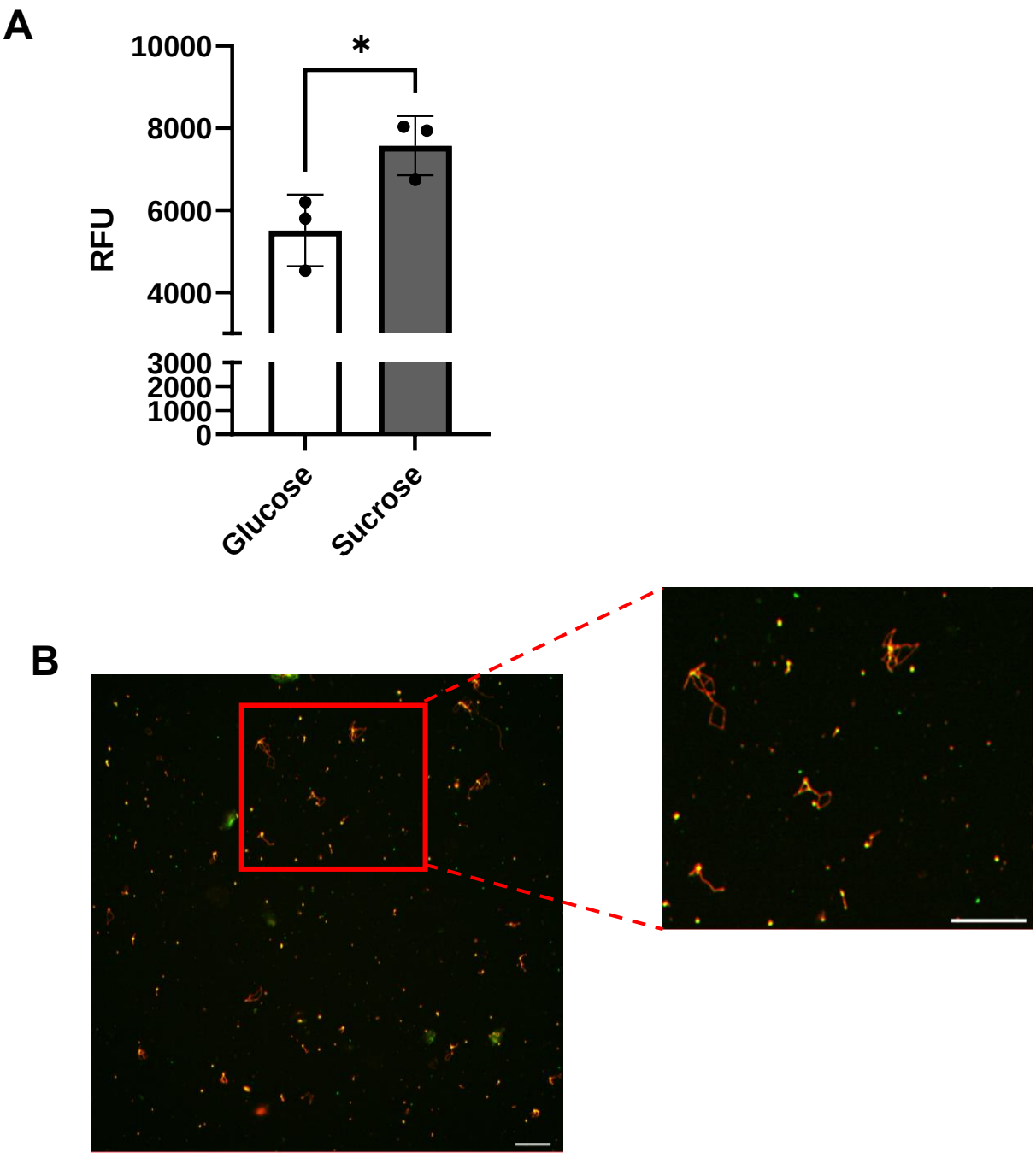


**Figure 6: Glucans co-localise with eDNA structures.** WT *S. gordonii* biofilms were grown on saliva-coated 24-well plates for 5 h at 37 °C in YPT ± 0.2% glucose/sucrose. (A) Relative levels of glucans were measured following application of dextran Alexa Fluor™ 647 conjugated antibody. Data are presented as mean ± SD. *P<0.05, as determined via Student's t-test (n = 3). (B) eDNA stranding (red) and glucans (green) in the presence of sucrose were assessed via microscopy. Yellow indicates co-localisation. Representative image; scale bars, 50 µm.

312

### *Effects of DNase, SsnA, on eDNA networks*

Application of exogenous nuclease enzymes has been shown to disrupt eDNA networks within biofilms (42, 43). Nuclease enzymes are also expressed by several bacterial species, but little is known about their capacity to modulate biofilm eDNA. Previous studies had identified the nuclease activity of *S. gordonii* and we have characterised this enzyme as Streptococcal Surface Nuclease A (SsnA) (44). We therefore generated a Δ*ssnA* mutant strain and utilised our imaging system to determine if SsnA can influence eDNA network formation during *S. gordonii* biofilm development. Levels of eDNA for Δ*ssnA* biofilms were 2.3-fold greater than those observed for *S. gordonii* WT biofilms (Fig. 7A), while total biomass levels (Fig. 7B) and eDNA matrix architecture (Fig. S2) were comparable. This suggested that SsnA can influence *S. gordonii* eDNA levels and may have the capacity to manipulate or disperse eDNA networks as the biofilm develops. These studies were then extended to monitor the effects of SsnA in glucose or sucrose environments, since nuclease activity can be regulated by carbon catabolite availability (45, 46). Addition of glucose resulted in eDNA levels that were comparable to the Δ*ssnA* mutant in the absence of sugars and, as before, higher levels of eDNA were seen in the presence of sucrose. However, for both sugars, these effects were independent of SsnA, as no significant differences were seen for eDNA or biomass between the Δ*ssnA* mutant and *S. gordonii* WT (Fig. 7A,B). One potential explanation for this effect was that utilisation of the sugars via glycolysis and concomitant production of lactic acid, reduced the local pH to below the activity threshold for SsnA. To explore this, the pH of the culture media ± sugar supplementation following biofilm formation

was measured. For both glucose and sucrose, it was confirmed that pH levels fell below pH 7.0, which would have reduced SsnA activity (Table 3).

As a final assessment of the capacity for SsnA to modulate eDNA networks, recombinant SsnA (rSsnA) was applied to biofilms formed by *S. gordonii* WT and Δ*ssnA* strains (Fig. 7C,D). As before, no significant differences were seen in total biomass levels between the two strains (Fig. 7D). By contrast, while exogenous SsnA had no impact on the levels of eDNA for WT *S. gordonii* biofilms, the enhanced eDNA stranding levels seen for Δ*ssnA* biofilms were diminished and restored to WT levels following application of rSsnA (Fig. 7C). These data provide further evidence of a role for SsnA in manipulating the eDNA networks of *S. gordonii* biofilms under conditions permissive to enzymatic activity.

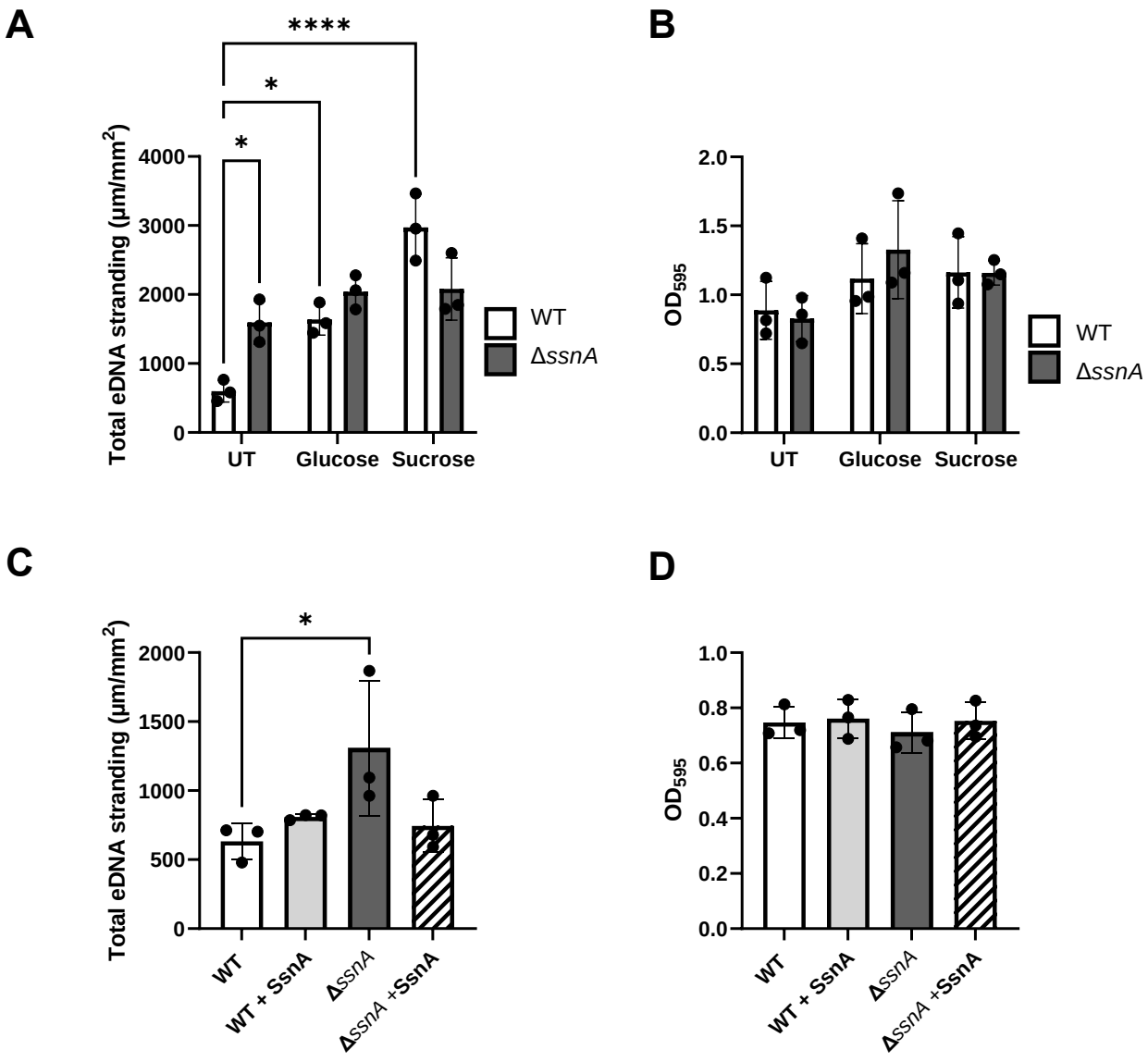


**Figure 7: SsnA can modulate eDNA levels but is affected by carbon source.** *S. gordonii* WT and ΔssnA biofilms were grown on saliva-coated 24-well plates for 5 h at 37 °C in YPT in the absence (UT) or presence of 0.2% glucose/sucrose. eDNA stranding (A) and levels of biomass (B) were determined by microscopy or crystal violet staining, respectively. S. gordonii WT and ΔssnA biofilms were also grown ± 5 µg/ml SsnA and eDNA stranding (C) and biomass (D) were determined as above. Data are presented as mean ± SD (n = 3). *P<0.05 and ***P<0.001, as determined via one-way ANOVA followed by Tukey test.

346

### *Modulation of eDNA networks via competence and Hpp systems*

A number of studies have implicated the competence (*comCDE*) system in regulating eDNA release by *S. gordonii* (16-18, 47). We therefore used our imaging system to verify the modulatory effects of the competence system on eDNA networks within *S. gordonii* biofilms. A panel of knockout mutants defective in different stages of the competence pathway were utilised for these studies: Δ*comC* (cannot express CSP), Δ*comDE* (expresses but cannot detect CSP), Δ*comCDE* (cannot express or detect CSP) and Δ*comR1/R2* (cannot upregulate competence genes in response to CSP). Biomass levels were comparable for biofilms formed by all the strains tested (Fig. 8B). By contrast, relative to WT, biofilms formed by strains Δ*comC*, Δ*comCDE* and Δ*comR1/R2* exhibited significantly lower levels of eDNA, with reductions of 56%, 83% and 68%, respectively (Fig. 8A). This confirmed the proposed role of competence genes in mediating *S. gordonii* eDNA release and of CSP as the signal to induce these effects. Unexpectedly, however, eDNA levels for Δ*comDE* biofilms were comparable to those of WT, despite the absence of the cognate two-component signal system (ComDE) to detect the CSP signal (Fig. 8A). This suggested that *S. gordonii* may be utilising an alternative mechanism to detect CSP and this hypothesis was further supported by complementation studies using exogenous CSP (Fig. 8C). As was anticipated, application of exogenous CSP to Δ*comC* biofilms restored eDNA networks to WT levels (Fig. 8C). No effect was seen for the already higher eDNA levels of WT and Δ*comDE* biofilms. However, a significant (6-fold) increase was also seen in eDNA following application of exogenous CSP to Δ*comCDE* biofilms, despite lacking the ComDE CSP detection apparatus (Fig. 8C). Importantly, this response was specific to CSP, as no

such effect was seen following application of a scrambled CSP peptide as control (data not shown). Assessment of eDNA matrix architecture also revealed some variability in eDNA junction composition in competence mutants, relative to WT biofilm (Figures S4 – 5).

Another regulatory system that has been associated with competence in *S. gordonii* is the hexa-heptapeptide permease (Hpp) system (48). The Hpp system is an oligopeptide permease system comprising four constituents: HppA, HppB, HppG and HppH. HppA has been implicated in substrate specific binding and along with HppH, transports peptides comprising 5-7 amino acid residues across the cell envelope and into *S. gordonii* cells. To ascertain whether the Hpp system may have capacity to detect CSP in the absence of ComDE and so facilitate CSP modulation of eDNA networks, knockout mutants lacking HppA or HppH, individually or in combination with Δ*comCDE*, were generated and tested. Slight variations were seen in biofilm biomass levels across the strains but the addition of exogenous CSP had no significant effects (Fig. 9A,C). By contrast, biofilms formed by mutants lacking HppA or HppH were reduced in eDNA levels relative to WT and these were restored upon application of exogenous CSP (Fig. 9A,B). For biofilms formed by strains lacking ComCDE in addition to HppA or HppH, levels of eDNA were significantly lower than those for WT biofilms but addition of exogenous CSP had no effect (Fig. 9A,B). Interestingly, HppH biofilms exhibited diminished numbers of branches/junctions per eDNA structure (Figure S6). Indicating, the ability of HppH, but not HppA in modulating eDNA matrix architecture. Taken together, these data support the hypothesis that the Hpp system can engage CSP and

392 that via CSP detection, both the ComCDE and Hpp systems can modulate eDNA

393 networks within *S. gordonii* biofilms.

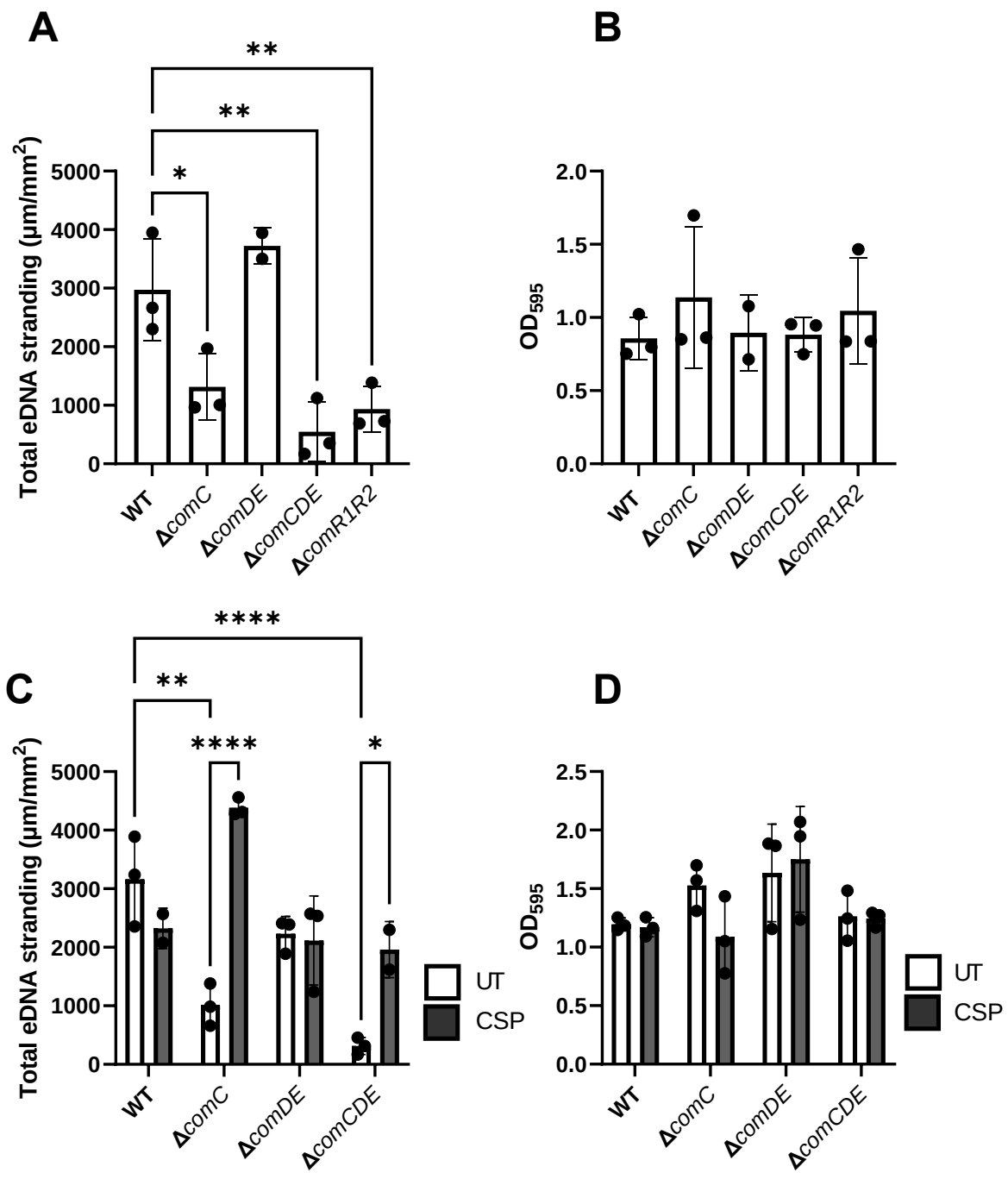


**Figure 8: CSP modulates eDNA stranding in *S. gordonii* biofilms, even in absence of ComDE apparatus**. WT *S. gordonii* and various *comCDE* operon mutant strains were grown at 37 °C in YPTG on saliva-coated 24-well plates ± CSP for 5 h. Levels of biomass and eDNA stranding (n = 3, Δ*comDE*; n = 2) were then determined by crystal violet staining or microscopy, respectively. Data are presented as mean ± SD. *P< 0.05, **P<0.01, ***P<0.001 or **** P< 0.0001, as determined by one way ANOVA followed by Tukey test.

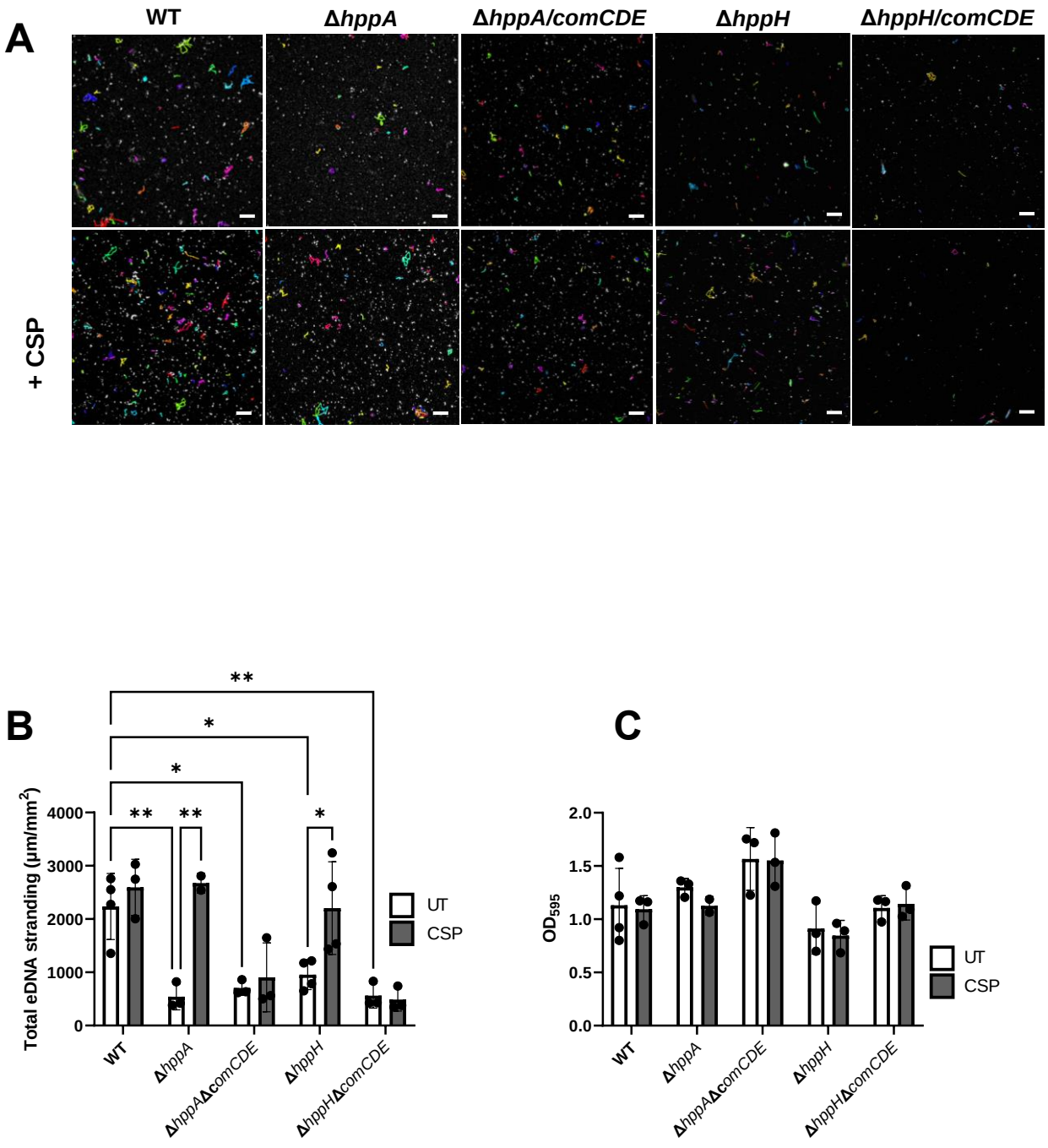


**Figure 9: Hpp system responds to CSP to modulate eDNA.** WT S. *gordonii* or *hpp* ± *comCDE* system mutants were grown at 37 °C in YPTG on saliva-coated 24-well plates ± 10 µg/ml CSP for 5 h. Levels of eDNA stranding (A,B) and biomass (C) were then determined by microscopy or crystal violet staining, respectively. (A) indicates representative images of eDNA stranding. Data are presented as mean ± SD. *P<0.05 or **P<0.01, as determined by two-way ANOVA followed by Tukey test; n = 3/4. Scale bars, 50 µm.

## Discussion

Advances in fluorescence microscopy techniques have provided novel insights into the architecture of eDNA networks, showing them to form “web-” or “lattice-like” structures across the biofilm (9, 10). However, studies requiring the quantification of eDNA have had to rely on the analysis of soluble eDNA, which is disconnected from this complex eDNA architecture. To address this gap, this study presents use of a high-throughput image analysis tool that enables the visualisation and quantification of eDNA networks *in situ* within biofilms. Furthermore, alongside quantification of eDNA abundance, this imaging platform provides the ability to interrogate the detail of eDNA networks with regards to, for example, eDNA branch length and number. Such high-level analysis of eDNA architecture has not previously been possible.

To validate the capacity of this imaging system to both reliably detect eDNA, and exhibit sufficient sensitivity to detect differences in abundance, the effects of DNase I and sugars were examined. As predicted, DNase I reduced total eDNA levels in a dose-dependent manner. Interestingly, eDNA still remained abundant following DNase I application. Which may be due to the abundance of Z-form DNA, which are abundant within eDNA matrices and recalcitrant to treatment with DNases (49). Additionally, eDNA matrices are stabilised by DNA binding proteins which may limit accessibility to eDNA structures by DNase enzymes (9, 12).

By contrast, the presence of sucrose promoted eDNA production relative to glucose. This correlates with the established role of $H_2O_2$ in regulating eDNA release by *S. gordonii* (47, 50). $H_2O_2$ production is governed by SpxB, which in turn is under the control of carbon catabolite regulator, CcpA (50). Moreover, these effects on eDNA

directly correlated with glucan production, with evidence that glucans may serve as a form of structural support for the eDNA networks. Where, the number of junctions within eDNA networks of sucrose biofilms were significantly diminished in the presence of dextranase or the absence of GtfG. Indicating, glucans may stabilise eDNA matrices at points where eDNA branches, serving a similar role as DNA binding proteins (9). This correlates with studies using *S. mutans*, for which eDNA has also been shown to increase in a glucan-dependent manner within biofilms (51-53). In which, GtfB expressed by *Streptococcus mutans* acts synergistically with eDNA to promote adherence to surfaces (54). With several *Streptococcus* species known to express Gtfs (55), glucan-mediated support of eDNA matrices may represent a common mechanism during biofilm development under conditions permissive to glucan production.

This study also demonstrated that surface associated nuclease SsnA of *S. gordonii* could modulate eDNA levels. SsnA has homology to SWAN of *S. sanguinis*, which has been shown to degrade neutrophil extracellular traps (20), but this is the first evidence of a surface-expressed nuclease influencing eDNA abundance, but not architecture, within biofilms. In the absence of SsnA, *S. gordonii* biofilms exhibited a greater abundance of eDNA networks, suggesting that SsnA may act directly on the eDNA strands to release or reorganise the networks. However, the impact of SsnA was significantly affected by conditions within the local environment. SsnA is only active in the pH range 7 - 10 (data not shown) and thus was rendered inactive in the presence of fermentable carbohydrate due to the resultant acidification of the environment from glycolysis. Nuclease enzyme expression has been observed from an array of oral biofilm commensals (44). As such, going forward, it will be interesting to determine the

contribution that surface-bound nucleases make to organisation of the eDNA matrices found within polymicrobial biofilms of the oral cavity and at other sites, and the implications of variations in eDNA architecture for overall biofilm properties.

It has been recognised for some time that the competence can regulate the release of eDNA by *S. gordonii* and *S. mutans* (4). During the competence pathway in *S. gordonii*, pre-CSP (encoded by *comC*) is a 50 aa polypeptide that is cleaved by ComA to produce the mature 19 aa CSP. Mature CSP is transported out of the cell by the ComAB ABC binding cassette transporter and detected by two-component system (TCS) ComDE. ComD autophosphorylates upon detection of CSP and phosphorylates its intracellular response regulator, ComE. ComE subsequently modulates expression of the competence-specific alternative σ factor, ComR, which regulates transcription of the competence genes, including murein hydrolase LytF, enabling the bacterial cell to take up DNA from the environment (24, 47). Specific to eDNA release, it has been proposed that detection of CSP induces upregulation of AtlS that, in turn, upregulates expression SpxB. This results in an increase in the intracellular concentration of $H_2O_2$, with the resultant oxidative stress ultimately inducing LytF expression and eDNA release (4). The data presented in this study support the role of CSP in eDNA release. Specifically, our image analysis system revealed that the abundance of eDNA within *S. gordonii* biofilms was significantly diminished in the absence of CSP. Unexpectedly, however, it was also revealed that detection of CSP was not dependent on ComDE. Rather, the data imply that the Hpp system can serve as an alternative system for CSP detection and subsequent induction of downstream gene regulation. Cells lacking ComDE but with an intact Hpp system could respond to exogenous CSP, with a concomitant

increase in eDNA abundance. Importantly, this was a specific effect, as no such elevation in eDNA levels was seen using a scrambled CSP peptide. Production of eDNA could not be rescued by the application of exogenous CSP to cells lacking both the ComDE and HppA/H detection apparatus, indicating that the cross-talk does not extend beyond these two systems.

As Hpp has been described as a hexa-heptapeptide permease system (48), it is yet to be understood how the 19 aa CSP can be detected. It is possible that some form of extracellular interaction causes signal transduction, without requiring full CSP entry to the cell. For example, for bacteria such as *Lactococcus lactis,* the Opp family proteins have been shown to detect peptides between 4-35 aa in length, as the whole peptide does not enter the recognition site of OppA (homologous to HppA in *S. gordonii*) (48, 56). Alternatively, CSP may be cleaved to a shorter length peptide prior to translocation into the cell via the Hpp system. In *S. mutans*, the 17 aa peptide ComS is processed at a double tryptophan motif (WW), releasing a 7 aa SigX inducing peptide (XIP) that is imported into the cell via an Opp system (57). As the mature *S. gordonii* CSP also possesses a WW motif, it is possible that this peptide may be processed in a similar way for recognition via the Hpp system. Exploring such possibilities will be the focus of future studies.

In summary, by exploiting our high-throughput image analysis tool, this study has provided a more detailed understanding of the factors that can modulate eDNA networks within *S. gordonii* biofilms. Evidence is provided of the capacity for glucans to stabilise eDNA matrices, while surface-bound nuclease SsnA has been shown to modify these structures under conditions permissive for enzymatic activity. Furthermore, while

the role of CSP in inducing eDNA release is confirmed, a more complex regulatory mechanism has been revealed, with cross-talk with the Hpp system evident. Extending beyond *S. gordonii*, a critical feature of this imaging system is its capacity to discriminate between eDNA strands, allowing a detailed quantification of the eDNA architecture *in situ* within biofilms that has not before been possible. Results obtained revealed that aspects of eDNA architecture including average branch length remained consistent across all experiments, but other features including junctional composition were highly variable.

Going forward, this can be exploited across the field of biofilm research to enable high level interrogation of exactly how eDNA networks develop, how these networks contribute to the properties of the biofilm, and how this can be modulated. However, a current limitation to this technique is the use of an antibody that only recognises dsDNA structures. As, eDNA matrices are abundant in Z-form DNA structures and stabilised by DNA binding proteins that may mask eDNA structures (9, 49). Future studies should endeavour to develop techniques to detect these structures. Such opportunities should significantly advance attempts to disrupt eDNA matrices within biofilms for therapeutic benefit, including oral biofilms.

**Acknowledgements**

This research in this report is funded by the Dunhill Medical Trust (RPGF1810\101). We acknowledge support from the Wolfson Bioimaging Facility and BrisSynBio, a BBSRC/EPSRC-funded Synthetic Biology Research Centre (grant number: L01386X). The authors declare no potential conflicts of interest with respect to the authorship and/or publication of this article

511 **Table 1**: Strains used in this study

| Identifier | Strain | Relevant Characteristics | Ref |
|---|---|---|---|
| UB1507 | DL1 (Challis) | Parental Strain | (58) |
| UB653 | Δ*gtfG* | *gtfG*::*aad9* | (59) |
| UB2660 | Δ*comC* | *comC*::*aad9* | (24) |
| UB2661 | Δ*comDE* | *comCD*::*aad9* | This study |
| UB2347 | Δ*comCDE* | *comCDE*::*aad9* | (24) |
| UB2975 | Δ*comR1R2* | *comR1::aad9 comR2::ermAM* | This study |
| UB2953 | Δ*hppA* | *hppA::ermAM* | This study |
| UB2958 | Δ*hppA* Δ*comCDE* | *hppA::ermAM comCDE*::*aad9* | This study |
| UB3097 | Δ*hppH* | *hppH::aphA3* | This study |
| UB3098 | Δ*hppH* Δ*comCDE* | *hppH::aphA3 comCDE*::*aad9* | This study |
| UB2886 | Δ*ssnA* | *ssnA::aad9* | Rostami et al |

512

513

514 **Table 2** Primers used in this study

| **Mutant generated** | **Primer name** | **Primer sequence** | **Function** |
|---|---|---|---|
| Δ*ssnA* | *SsnA.F1*<br>*SsnA.R1* | TTTTATCAGAAATTGATTG<br>AAAGTTCTCCTTTTCCTA | Amplify 484-bp amplicon upstream of *ssnA* |
| | *SsnA.F2*<br>*SsnA.R2* | CCTAGAGTAAGCTCTAAACA<br>TGTCAAAGCTACCAGTAC | Amplify 674-bp amplicon downstream of *ssnA* |
| | aad9_SsnAF<br>aad9_SsnAR | AGGAGAACTTTATGAATACATACGAACAAATTAATA<br>GCTTACTCTCTAGGTTATAATTTTTTTAATCTGTTATTTAA | Amplify 782-bp *aad9* cassette from pFW5 with overlaps for *ssnA* flanking regions |
| Δ*comDE* | *ComCD.F1*<br>*ComDE.R1* | CGACTCAGTCGTTTTACGAAAG<br>GGAGATTGAAATGATATTTACAATGGATCCGACAAAG | Amplify 448-bp amplicon upstream of *comDE* |

| | | | |
|---|---|---|---|
| | *ComDE.F1*<br><br>*ComCDE.R2* | TTACAATGGATCCGACAAAGCGAGATAAACTGG<br><br>CTACTTCGCGGATATTGGC | Amplify 619-bp amplicon downstream of *comDE* |
| | *ComDE_Aad9F*<br><br>*ComDE_Aad9R* | GGAGATATTTTTTTGAATACATACGAACAAATT<br><br>GTTAGAGGATTTTAATATTAAAAAAATTAGACAATAAAT | Amplify 1100-bp *aad9* cassette from pFW5 with overlaps for *comDE* flanking regions |
| Δ*comR1* | *ComR1.F1*<br><br>*ComR1.R1* | GATATTCCAGGATCCTGCTG<br><br>TATGTATTCATTGACTAGTCCTTTCTTTTTG | Amplify 586-bp amplicon upstream of *comR1* |
| | *ComR1.F2*<br><br>*ComR1.R2* | AAAAAATTATAAAAAGAAGGGAGAGGCAATC<br><br>CCTCAGCGTCAGTTACAGAC | Amplify 1075-bp amplicon downstream of *comR1* |
| | *aad9.comr1F* | GACTAGTCAATGAATACATACGAACAAATTAATA | Amplify 770-bp *aad9* cassette from pFW5 with |

| | | | |
|---|---|---|---|
| | *aad.comR1 R* | CCTTCTTTTTATAATTTTTTTAATCTGTTATTTAA | overlaps for *comR1* flanking regions |
| *∆comR2* | *ComR2.F1*<br>*ComR2.R1* | TCCAGGTGCATATAATCCAC<br>ATTTTTGTTCATTGACTAGTCCTTTCTTTTTG | Amplify 840-bp amplicon upstream of *comR2* |
| | *ComR2.F2*<br>*ComR2.R2* | GGAGGAAATAAAAAGAAGGGAGAGGCAATC<br>CCTCAGCGTCAGTTACAGAC | Amplify 1075-bp amplicon upstream of *comR2* |
| | *ermAM.comR2F*<br>*ermAM.comR2R* | ACTAGTCAATGAACAAAAATATAAAATATTCTCAAAAC<br>CCCTTCTTTTTATTTCCTCCCGTTAAATAATAG | Amplify 755-bp *ermAM* cassette from pVA838 with overlaps for *comR2* flanking regions |
| *∆hppA* | *HppA.F1*<br>*HppA.R1* | CAACAATCCAGACCAATACTC<br>GAAATGGAGAATATACGATGAACAAAAA | Amplify 953-bp amplicon upstream of *hppA.* |

| | | | |
|---|---|---|---|
| | *HppA.F2*<br><br>*HppA.R2* | CGGGAGGAAATAACCAATCATTAGA ACTTTC<br><br>CCATCCATGCTTGTTAGC | Amplify 932-bp amplicon downstream of *hppA* |
| | *ermAM.hpp AF*<br><br>*ermAM.hpp AR* | AATATACGATGAACAAAAATATAAAA TATTCTC<br><br>TGATTGGTTATTTCCTCCCGTTAAAT A | Amplify 753-bp *ermAM* cassette from pVA838 with overlaps for *comR2* flanking regions |
| ∆*hppH* | *HppH.F1*<br><br>*HppH.R1* | CCCGATTCACTTAGATCTTC<br><br>CATTTTAGCCATGAAATACTCCTTTC AAAATA | Amplify 901-bp amplicon upstream of *hppH* |
| | *HppH.F2*<br><br>*HppH.R2* | ATTGTTTTAGCAATTACCCTAACGAG GAGG<br><br>GATACTTGTCGGGTCAGTAGC | Amplify 906-bp amplicon upstream of *hppH.* |
| | *aphA3.hppH F* | AGTATTTCATGGCTAAAATGAGAATA TCACC | Amplify 813-bp *aphA3* cassette from pDL276 with overlaps for |

| | | | |
|---|---|---|---|
| | *aphA3.hppHR* | AGGGTAATTGCTAAAACAATTCATCCAGTAAAATA | *comR2* flanking regions |

**Table 3:** Media pH of 5 h biofilms

| | Strain | pH* |
|---|---|---|
| **Untreated** | WT | 7.11 ± 0.03 |
| | WT + SsnA | 7.18 ± 0.06 |
| | *ΔssnA* | 7.16 ± 0.11 |
| | *ΔssnA* + SsnA | 7.15 ± 0.11 |
| **0.2% Glucose** | WT | 6.85 ± 0.06 |
| | *ΔssnA* | 6.84 ± 0.10 |
| **0.2% Sucrose** | WT | 6.26 ± 0.09 |
| | *ΔssnA* | 6.66 ± 0.11 |

*Data is presented as mean ± SD, n = 8.

## References


1. Jakubovics NS, Grant Burgess J. Extracellular DNA in oral microbial biofilms. Microbes and Infection. 2015;17(7):531-7.
2. Nagler M, Insam H, Pietramellara G, Ascher-Jenull J. Extracellular DNA in natural environments: features, relevance and applications. Applied microbiology and biotechnology. 2018;102(15):6343-56.
3. Dadon Z, Cohen A, Szterenlicht YM, Assous MV, Barzilay Y, Raveh-Brawer D, et al. Spondylodiskitis and endocarditis due to Streptococcus gordonii. Ann Clin Microbiol Antimicrob. 2017;16(1):68.
4. Serrage HJ, Jepson MA, Rostami N, Jakubovics NS, Nobbs AH. Understanding the Matrix: The Role of Extracellular DNA in Oral Biofilms. Frontiers in Oral Health. 2021;2(7).
5. Jamal M, Ahmad W, Andleeb S, Jalil F, Imran M, Nawaz MA, et al. Bacterial biofilm and associated infections. J Chin Med Assoc. 2018;81(1):7-11.
6. Dengler V, Foulston L, DeFrancesco AS, Losick R. An electrostatic net model for the role of extracellular DNA in biofilm formation by Staphylococcus aureus. Journal of Bacteriology. 2015;197(24):3779-87.
7. Kavanaugh JS, Flack CE, Lister J, Ricker EB, Ibberson CB, Jenul C, et al. Identification of Extracellular DNA-Binding Proteins in the Biofilm Matrix. mBio. 2019;10(3).
8. Seviour T, Winnerdy FR, Wong LL, Shi X, Mugunthan S, Foo YH, et al. The biofilm matrix scaffold of Pseudomonas aeruginosa contains G-quadruplex extracellular DNA structures. npj Biofilms and Microbiomes. 2021;7(1):27.
9. Devaraj A, Buzzo JR, Mashburn-Warren L, Gloag ES, Novotny LA, Stoodley P, et al. The extracellular DNA lattice of bacterial biofilms is structurally related to Holliday junction recombination intermediates. Proceedings of the National Academy of Sciences. 2019;116(50):25068.
10. Barnes AMT, Ballering KS, Leibman RS, Wells CL, Dunnya GM. Enterococcus faecalis produces abundant extracellular structures containing DNA in the absence of cell lysis during early biofilm formation. mBio. 2012;3(4).
11. Devaraj A, Justice SS, Bakaletz LO, Goodman SD. DNABII proteins play a central role in UPEC biofilm structure. Molecular Microbiology. 2015;96(6):1119-35.
12. Devaraj A, Buzzo J, Rocco CJ, Bakaletz LO, Goodman SD. The DNABII family of proteins is comprised of the only nucleoid associated proteins required for nontypeable Haemophilus influenzae biofilm structure. MicrobiologyOpen. 2018;7(3).
13. Rocco CJ, Bakaletz LO, Goodman SD. Targeting the HUβ protein prevents Porphyromonas gingivalis from entering into preexisting biofilms. Journal of Bacteriology. 2018;200(11).
14. Rocco CJ, Davey ME, Bakaletz LO, Goodman SD. Natural antigenic differences in the functionally equivalent extracellular DNABII proteins of bacterial biofilms provide a means for targeted biofilm therapeutics. Molecular Oral Microbiology. 2017;32(2):118-30.
15. Loo CY, Corliss DA, Ganeshkumar N. Streptococcus gordonii biofilm formation: identification of genes that code for biofilm phenotypes. Journal of bacteriology. 2000;182(5):1374-82.
16. Kreth J, Vu H, Zhang Y, Herzberg MC. Characterization of hydrogen peroxide-induced DNA release by Streptococcus sanguinis and Streptococcus gordonii. Journal of Bacteriology. 2009;191(20):6281-91.
17. Xu Y, Kreth J. Role of LytF and AtlS in eDNA Release by Streptococcus gordonii. PLoS ONE. 2013;8(4).
18. Itzek A, Zheng L, Chen Z, Merritt J, Kreth J. Hydrogen peroxide-dependent DNA release and transfer of antibiotic resistance genes in Streptococcus gordonii. Journal of Bacteriology. 2011;193(24):6912-22.

19. Dutton LC, Nobbs AH, Jepson K, Jepson MA, Vickerman MM, Aqeel Alawfi S, et al. O-mannosylation in Candida albicans enables development of interkingdom biofilm communities. mBio. 2014;5(2):e00911-e.
20. Morita C, Sumioka R, Nakata M, Okahashi N, Wada S, Yamashiro T, et al. Cell Wall-Anchored Nuclease of Streptococcus sanguinis Contributes to Escape from Neutrophil Extracellular Trap-Mediated Bacteriocidal Activity. PLOS ONE. 2014;9(8):e103125.
21. Podbielski A, Spellerberg B, Woischnik M, Pohl B, Lütticken R. Novel series of plasmid vectors for gene inactivation and expression analysis in group A streptococci (GAS). Gene. 1996;177(1-2):137-47.
22. Shimell MJ, Smith CJ, Tally FP, Macrina FL, Malamy MH. Hybridization studies reveal homologies between pBF4 and pBFTM10, Two clindamycin-erythromycin resistance transfer plasmids of Bacteroides fragilis. Journal of bacteriology. 1982;152(2):950-3.
23. Dunny GM, Lee LN, LeBlanc DJ. Improved electroporation and cloning vector system for gram-positive bacteria. Applied and environmental microbiology. 1991;57(4):1194-201.
24. Jack AA, Daniels DE, Jepson MA, Margaret Vickerman M, Lamont RJ, Jenkinson HF, et al. Streptococcus gordonii comCDE (competence) operon modulates biofilm formation with Candida albicans. Microbiology (United Kingdom). 2015;161(2):411-21.
25. Rueden CT, Schindelin J, Hiner MC, DeZonia BE, Walter AE, Arena ET, et al. ImageJ2: ImageJ for the next generation of scientific image data. BMC Bioinformatics. 2017;18(1):529.
26. Schindelin J, Arganda-Carreras I, Frise E, Kaynig V, Longair M, Pietzsch T, et al. Fiji: an open-source platform for biological-image analysis. Nature Methods. 2012;9(7):676-82.
27. Cross S. MIA: Version 0.11.2. Zenodo. 2019.
28. Steger C. An unbiased detector of curvilinear structures. IEEE Transactions on Pattern Analysis and Machine Intelligence. 1998;20(2):113-25.
29. Wagner T. Ridge Detection v1.4.0. Zenodo. 2017.
30. Arganda-Carreras I, Fernández-González R, Muñoz-Barrutia A, Ortiz-De-Solorzano C. 3D reconstruction of histological sections: Application to mammary gland tissue. Microsc Res Tech. 2010;73(11):1019-29.
31. Jin Y, Guo Y, Zhan Q, Shang Y, Qu D, Yu F. Subinhibitory concentrations of mupirocin stimulate Staphylococcus aureus biofilm formation by upregulating cidA. Antimicrobial Agents and Chemotherapy. 2020;64(3).
32. Yuan Z, Dai Y, Ouyang P, Rehman T, Hussain S, Zhang T, et al. Thymol inhibits biofilm formation, eliminates pre‐existing biofilms, and enhances clearance of methicillin‐resistant Staphylococcus aureus (MRSA) in a mouse peritoneal implant infection model. Microorganisms. 2020;8(1).
33. Padmavathi AR, Periyasamy M, Pandian SK. Assessment of 2,4-Di-tert-butylphenol induced modifications in extracellular polymeric substances of Serratia marcescens. Bioresource Technology. 2015;188:185-9.
34. Zheng L, Chen Z, Itzek A, Ashby M, Kreth J. Catabolite control protein a controls hydrogen peroxide production and cell death in streptococcus sanguinis. Journal of Bacteriology. 2011;193(2):516-26.
35. Gilmore KS, Srinivas P, Akins DR, Hatter KL, Gilmore MS. Growth, development, and gene expression in a persistent Streptococcus gordonii biofilm. Infection and immunity. 2003;71(8):4759-66.
36. Zheng L, Itzek A, Chen Z, Kreth J. Environmental influences on competitive hydrogen peroxide production in Streptococcus gordonii. Applied and environmental microbiology. 2011;77(13):4318-28.
37. Li Y, Du Y, Ye J, Wang B, Liu Y. Effect of extracellular DNA on the formation of Streptococcus mutans biofilm under sucrose environment. Zhonghua kou qiang yi xue za zhi = Zhonghua kouqiang yixue zazhi = Chinese journal of stomatology. 2016;51(2):81-6.

626 38. Kim M, Jeon J, Kim J. Streptococcus mutans extracellular DNA levels depend on the number of
627 bacteria in a biofilm. Scientific Reports. 2018;8(1):13313.
628 39. Koo H, Xiao J, Klein MI, Jeon JG. Exopolysaccharides produced by Streptococcus mutans
629 glucosyltransferases modulate the establishment of microcolonies within multispecies biofilms. Journal
630 of bacteriology. 2010;192(12):3024-32.
631 40. Vickerman MM, Jones GW, Clewell DB. Molecular analysis of representative Streptococcus
632 gordonii Spp phase variants reveals no differences in the glucosyltransferase structural gene, gtfG. Oral
633 Microbiol Immunol. 1997;12(2):82-90.
634 41. Vickerman MM, Minick PE. Genetic analysis of the rgg-gtfG junctional region and its role in
635 Streptococcus gordonii glucosyltransferase activity. Infect Immun. 2002;70(4):1703-14.
636 42. Rostami N, Shields RC, Yassin SA, Hawkins AR, Bowen L, Luo TL, et al. A Critical Role for
637 Extracellular DNA in Dental Plaque Formation. Journal of Dental Research. 2017;96(2):208-16.
638 43. Brown HL, Reuter M, Hanman K, Betts RP, Van Vliet AHM. Prevention of biofilm formation and
639 removal of existing biofilms by extracellular dnases of campylobacter jejuni. PLoS ONE. 2015;10(3).
640 44. Palmer LJ, Chapple IL, Wright HJ, Roberts A, Cooper PR. Extracellular deoxyribonuclease
641 production by periodontal bacteria. J Periodontal Res. 2012;47(4):439-45.
642 45. Doke M, Fukamachi H, Morisaki H, Arimoto T, Kataoka H, Kuwata H. Nucleases from Prevotella
643 intermedia can degrade neutrophil extracellular traps. Molecular oral microbiology. 2017;32(4):288-300.
644 46. Kiedrowski MR, Kavanaugh JS, Malone CL, Mootz JM, Voyich JM, Smeltzer MS, et al. Nuclease
645 Modulates Biofilm Formation in Community-Associated Methicillin-Resistant Staphylococcus aureus.
646 PLOS ONE. 2011;6(11):e26714.
647 47. Zheng L, Chen Z, Itzek A, Herzberg MC, Kreth J. CcpA regulates biofilm formation and
648 competence in Streptococcus gordonii. Molecular oral microbiology. 2012;27(2):83-94.
649 48. Jenkinson HF, Baker RA, Tannock GW. A binding-lipoprotein-dependent oligopeptide transport
650 system in Streptococcus gordonii essential for uptake of hexa- and heptapeptides. Journal of
651 bacteriology. 1996;178(1):68-77.
652 49. Buzzo JR, Devaraj A, Gloag ES, Jurcisek JA, Robledo-Avila F, Kesler T, et al. Z-form extracellular
653 DNA is a structural component of the bacterial biofilm matrix. Cell. 2021;184(23):5740-58.e17.
654 50. Redanz S, Masilamani R, Cullin N, Giacaman RA, Merritt J, Kreth J. Distinct Regulatory Role of
655 Carbon Catabolite Protein A (CcpA) in Oral Streptococcal Expression. Journal of Bacteriology.
656 2018;200(8):e00619-17.
657 51. Li Y, Du Y, Ye J, Wang B, Liu Y. Effect of extracellular DNA on the formation of Streptococcus
658 mutans biofilm under sucrose environment. Chinese journal of stomatology. 2016;51(2):81-6.
659 52. Klein MI, DeBaz L, Agidi S, Lee H, Xie G, Lin AHM, et al. Dynamics of Streptococcus mutans
660 Transcriptome in Response to Starch and Sucrose during Biofilm Development. PLOS ONE.
661 2010;5(10):e13478.
662 53. Nagasawa R, Sato T, Senpuku H. Raffinose induces biofilm formation by Streptococcus mutans in
663 low concentrations of sucrose by increasing production of extracellular DNA and fructan. Applied and
664 Environmental Microbiology. 2017;83(15).
665 54. Liao S, Klein MI, Heim KP, Fan Y, Bitoun JP, Ahn S-J, et al. Streptococcus mutans extracellular
666 DNA is upregulated during growth in biofilms, actively released via membrane vesicles, and influenced
667 by components of the protein secretion machinery. Journal of bacteriology. 2014;196(13):2355-66.
668 55. Xu R-R, Yang W-D, Niu K-X, Wang B, Wang W-M. An Update on the Evolution of
669 Glucosyltransferase (Gtf) Genes in Streptococcus. Frontiers in Microbiology. 2018;9.
670 56. Lamarque M, Charbonnel P, Aubel D, Piard JC, Atlan D, Juillard V. A multifunction ABC
671 transporter (Opt) contributes to diversity of peptide uptake specificity within the genus Lactococcus. J
672 Bacteriol. 2004;186(19):6492-500.

673 57. Mashburn-Warren L, Morrison DA, Federle MJ. A novel double-tryptophan peptide pheromone
674 controls competence in Streptococcus spp. via an Rgg regulator. Mol Microbiol. 2010;78(3):589-606.
675 58. Vickerman MM, Iobst S, Jesionowski AM, Gill SR. Genome-wide transcriptional changes in
676 Streptococcus gordonii in response to competence signaling peptide. J Bacteriol. 2007;189(21):7799-
677 807.
678 59. Vickerman MM, Wang M, Baker LJ. An amino acid change near the carboxyl terminus of the
679 Streptococcus gordonii regulatory protein Rgg affects its abilities to bind DNA and influence expression
680 of the glucosyltransferase gene gtfG. Microbiology (Reading). 2003;149(Pt 2):399-406.

681